

3 ω correction method for eliminating resistance measurement error due to Joule heating ^{EP}

Cite as: Rev. Sci. Instrum. **92**, 094711 (2021); <https://doi.org/10.1063/5.0063998>

Submitted: 19 July 2021 • Accepted: 06 September 2021 • Published Online: 29 September 2021

 Benny Guralnik,  Ole Hansen, Henrik H. Henrichsen, et al.

COLLECTIONS

 This paper was selected as an Editor's Pick



View Online



Export Citation



CrossMark

ARTICLES YOU MAY BE INTERESTED IN

[Beam power scale-up in micro-electromechanical systems based multi-beam ion accelerators](#)

Review of Scientific Instruments **92**, 103301 (2021); <https://doi.org/10.1063/5.0058175>

[Determination of the temperature coefficient of resistance from micro four-point probe measurements](#)

Journal of Applied Physics **129**, 165105 (2021); <https://doi.org/10.1063/5.0046591>

[Projection-type electron spectroscopy collimator analyzer for charged particles and x-ray detections](#)

Review of Scientific Instruments **92**, 073301 (2021); <https://doi.org/10.1063/5.0051114>

Lock-in Amplifiers
up to 600 MHz



Zurich
Instruments



3ω correction method for eliminating resistance measurement error due to Joule heating

Cite as: Rev. Sci. Instrum. 92, 094711 (2021); doi: 10.1063/5.0063998

Submitted: 19 July 2021 • Accepted: 6 September 2021 •

Published Online: 29 September 2021



















View Online



Export Citation



CrossMark

Benny Guralnik,^{1,2,a)}  Ole Hansen,²  Henrik H. Henrichsen,¹ Braulio Beltrán-Pitarch,² 
Frederik W. Østerberg,¹  Lior Shiv,¹ Thomas A. Marangoni,²  Andreas R. Stilling-Andersen,² 
Alberto Cagliani,¹  Mikkel F. Hansen,¹  Peter F. Nielsen,¹  Herman Oprins,³  Bjorn Vermeersch,³ 
Christoph Adelman,³  Shibesh Dutta,³  Kasper A. Borup,⁴  Besira M. Mihiretie,⁵ 
and Dirch H. Petersen² 

AFFILIATIONS

¹CAPRES – A KLA Company, Diplomvej 373, 2800 Kgs. Lyngby, Denmark

²Technical University of Denmark, DK-2800 Kgs. Lyngby, Denmark

³Imec, Kapeldreef 75, B-3001 Leuven, Belgium

⁴Department of Chemistry, Aarhus University, Langelandsgade 140, DK-8000 Aarhus C, Denmark

⁵Hot Disk AB, SE-41288 Gothenburg, Sweden

^{a)} Author to whom correspondence should be addressed: benny.guralnik@gmail.com

ABSTRACT

Electrical four-terminal sensing at (sub-)micrometer scales enables the characterization of key electromagnetic properties within the semiconductor industry, including materials' resistivity, Hall mobility/carrier density, and magnetoresistance. However, as devices' critical dimensions continue to shrink, significant over/underestimation of properties due to a by-product Joule heating of the probed volume becomes increasingly common. Here, we demonstrate how self-heating effects can be quantified and compensated for via 3ω signals to yield zero-current transfer resistance. Under further assumptions, these signals can be used to characterize selected thermal properties of the probed volume, such as the temperature coefficient of resistance and/or the Seebeck coefficient.

© 2021 Author(s). All article content, except where otherwise noted, is licensed under a Creative Commons Attribution (CC BY) license (<http://creativecommons.org/licenses/by/4.0/>). <https://doi.org/10.1063/5.0063998>

I. INTRODUCTION

Here, we wish to introduce the 3ω technique^{1,2} into the context of micro-four-point probe (M4PP) electrical metrology,^{3–9} with the aim of improving the measurement accuracy of the latter via quantification and compensation for the so-called Self-Heating Effect (SHE).^{10,11} The undesirable heating associated with electrical micro-probing came to attention in the early 1960s, when the contact size between the metallic electrodes and the probed semiconductors dropped below ~ 0.1 μm .^{12–14} Since then, critical dimensions of semiconductor devices have shrunk by multiple orders of magnitude, while self-heating effects are often intentionally amplified.^{15,16} Thus, the elimination of undesirable by-products of heating in electrical microprobing has become increasingly relevant¹⁷ and is the main focus of the present contribution.

Traditionally, the unintentional generation of Joule heat during electrical microprobing has been mitigated via, e.g., measurement at sufficiently low^{14,18} or transient/pulsed currents¹⁷ and/or via optimization of the probing geometry.^{18,19} In a recent paradigm shift, we demonstrated⁹ that the seemingly undesired heating at such scales is highly reproducible and may be intentionally amplified in order to quantify the thermal properties of the material stack under test. Figure 1 summarizes the key highlights from Ref. 9, where an equidistant micro-four-point probe with a pitch of $10\ \mu\text{m}$ [Fig. 1(a)] was used to measure the sheet resistance of an ultrathin (16 nm) Pt film deposited on top of a fused silica substrate. The observed increase in the sheet resistance with the sampling current was proportional to the current squared in the 0.5–5 mA range [circles in Fig. 1(b), error bars within symbols]. A semianalytical approximation predicting this behavior was validated by finite element method

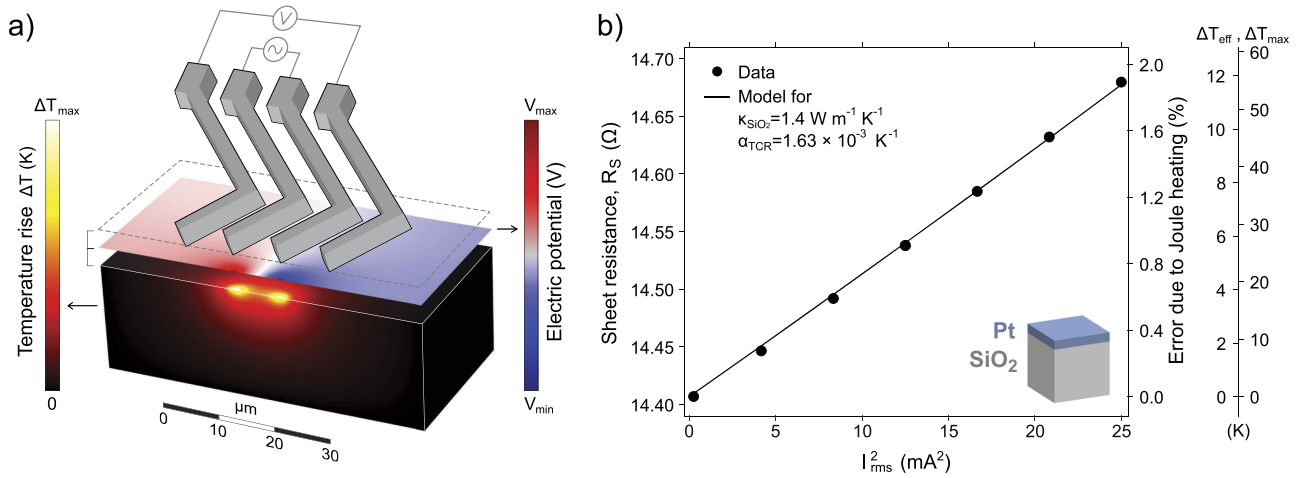


FIG. 1. The principle of TCR determination using the M4PP.⁹ (a) Numerical simulation (to scale) of a micro-four-point probe measurement of a Pt thin film on fused silica. The high current density in the vicinity of the two innermost, current-conducting electrodes results in surficial Joule heat and its conduction into the substrate (left color bar); in turn, locally elevated surface temperatures affect sheet resistivity, the electric field (right color bar), and ultimately, the effective sheet resistance. (b) The measured sheet resistance of Pt on fused silica (inset) increases linearly with squared rms current (\sim power), deviating from its idealized “zero-current” level by 1.9% at 5 mA. This trend can be numerically matched (line) via nonunique combinations of several thermal properties, in this case being the thermal conductivity of the substrate (presumed to be independently known) and the TCR of the thin film (designated as the unknown). Calculated for a presumed electric contact radius of 250 nm, the domain-averaged [Eq. (2)] and the maximum expected temperatures do also scale linearly with the current squared.

(FEM) simulations [continuous line in Fig. 1(b)]. Furthermore, by treating the thermal conductivity of the substrate as a known parameter, the temperature coefficient of resistance (TCR) of the thin film could be estimated with an excellent ($<2\%$) precision across multiple consecutive measurements (Table 1 in Ref. 9).

A classic correction for self-heating effects involves the extrapolation of the linear trend in Fig. 1(b) to zero current^{10,11} to obtain the heat-unaffected, “zero-current” resistance R_0 . However, such a correction requires two or more resistance measurements at well-separated currents. This requirement not only prolongs the measurement time but also exposes the target to potential irreversible changes at higher currents. Noting that mainstream M4PP metrology uses lock-in amplification (LIA) to reduce electrical noise,⁷ here we explore the possibility of estimating zero-current resistance by isolating and quantifying the thermally induced voltage component from higher voltage harmonics. Falling into the broad category of 1ω – 2ω – 3ω methods,² our particular M4PP measurement strategy and 3ω correction scheme are briefly outlined below.

II. THEORY

The following mathematical treatment is a recapitulation of Dames and Chen.² For further simplification, we shall assume a slowly varying measurement current (quasi-DC) such that any electrical and thermal lags (e.g., due to electrical and thermal capacitances) can be ignored. Thus, the location- and time-dependent temperature increment $\Delta T(\mathbf{r}, t)$ of the probed volume instantaneously follows the Joule heat dissipation distribution, which to first order can be expressed in terms of the position-dependent sample resistivity $\rho_0(\mathbf{r})$ and current density $\mathbf{J}(\mathbf{r}, t)$ as $\rho_0(\mathbf{r})|\mathbf{J}(\mathbf{r}, t)|^2$. Furthermore, using $\mathbf{J}(\mathbf{r}, t) = \mathbf{g}_r(\mathbf{r})I(t)$, where $I(t)$ is the instantaneous current and $\mathbf{g}_r(\mathbf{r})$ is the measurement geometry-dependent vector

function,²⁰ the instantaneous temperature increment can be written as $\Delta T(\mathbf{r}, t) = \psi(\mathbf{r})I^2(t)$. Note that $\psi(\mathbf{r})$ is a transfer function from the current squared into temperature, which explicitly depends only on the probing geometry (and implicitly on the material properties of the probed volume).

We shall assume a linearized resistivity model $\rho(\mathbf{r}, t) = \rho_0(\mathbf{r})[1 + \alpha\Delta T(\mathbf{r}, t)]$, where α is the temperature coefficient of resistivity (TCR), such that the instantaneous transfer resistance $R(t)$ becomes:

$$\begin{aligned} R(t) &= \int_{\Omega} \rho(\mathbf{r}, t) \hat{S}(\mathbf{r}) d\Omega \\ &= R_0 \left[1 + \alpha \frac{\int_{\Omega} \rho_0(\mathbf{r}) \Delta T(\mathbf{r}, t) \hat{S}(\mathbf{r}) d\Omega}{\int_{\Omega} \rho_0(\mathbf{r}) \hat{S}(\mathbf{r}) d\Omega} \right] \\ &= R_0 [1 + \alpha \Delta T_{\text{eff}}(t)]. \end{aligned} \quad (1)$$

Here, R_0 is the zero-current transfer resistance, and $\hat{S}(\mathbf{r})$ is the M4PP sensitivity to a local change in resistivity,^{9,20} which in this paper is defined as:

$$\hat{S}(\mathbf{r}) = \frac{\mathbf{J}(\mathbf{r}) \cdot \hat{\mathbf{J}}(\mathbf{r})}{\hat{I}}$$

where $\hat{\mathbf{J}}$ and \hat{I} are the hypothetical current density and intensity in an adjoint system with interchanged current and voltage assignments.^{9,20} The function $\Delta T_{\text{eff}}(t)$ is a domain-averaged “effective” temperature increment,^{2,9} which for M4PP may be expressed as

$$\Delta T_{\text{eff}}(t) = \left(\frac{\int_{\Omega} \rho_0(\mathbf{r}) \psi(\mathbf{r}) \hat{S}(\mathbf{r}) d\Omega}{\int_{\Omega} \rho_0(\mathbf{r}) \hat{S}(\mathbf{r}) d\Omega} \right) I^2(t) = \Psi I^2(t). \quad (2)$$

With this definition of Ψ as a domain-scaled and -averaged $\psi(\mathbf{r})$, the instantaneous transfer resistance becomes

$$R(t) = R_0 [1 + \alpha \Psi I^2(t)], \quad (3)$$

and the instantaneous measured voltage becomes

$$V(t) = R(t)I(t) = R_0I(t) + R_0\alpha\Psi I^3(t). \quad (4)$$

If we use a low-frequency sinusoidal measurement current at the angular frequency $\omega = 2\pi f$,

$$I(t) = I_0 \sin(\omega t), \quad (5)$$

the instantaneous measured voltage becomes

$$\begin{aligned} V(t) &= R_0I_0 \sin(\omega t) + R_0\alpha\Psi I_0^3 \sin^3(\omega t) \\ &= \left(R_0 + \frac{3}{4}R_0\alpha\Psi I_0^2\right)I_0 \sin(\omega t) + \left(-\frac{1}{4}R_0\alpha\Psi I_0^2\right)I_0 \sin(3\omega t) \\ &= R_{1\omega}I_0 \sin(\omega t) + R_{3\omega}I_0 \sin(3\omega t), \end{aligned} \quad (6)$$

where we have introduced the first and third harmonic resistances, defined as $R_{1\omega} = R_0 + \frac{3}{4}R_0\alpha\Psi I_0^2$ and $R_{3\omega} = -\frac{1}{4}R_0\alpha\Psi I_0^2$, respectively. Note that for a positive α , the expected third harmonic voltage phase

angle is $\varphi_{3\omega} = \pi$, making $R_{3\omega}$ negative; for a negative α , $\varphi_{3\omega} = 0$ and $R_{3\omega}$ is positive.

Equation (6) also shows that the zero-current transfer resistance R_0 can be recovered from harmonic resistances $R_{1\omega}$ and $R_{3\omega}$ by the simple calculation

$$R_0 = R_{1\omega} + 3R_{3\omega}. \quad (7)$$

The temperature coefficient of resistivity can then be calculated from

$$\alpha = \frac{-4R_{3\omega}}{R_0\Psi I_0^2} = \frac{-4R_{3\omega}}{(R_{1\omega} + 3R_{3\omega})\Psi I_0^2} = \frac{-4}{(R_{1\omega}/R_{3\omega} + 3)\Psi I_0^2}, \quad (8)$$

which is easily derived from Eqs. (6) and (7).

III. MATERIALS AND METHODS

A. Samples

In this study, we focus on four industrially relevant samples, including a metallic nanoscale interconnect [Fig. 2(a)], a metallic

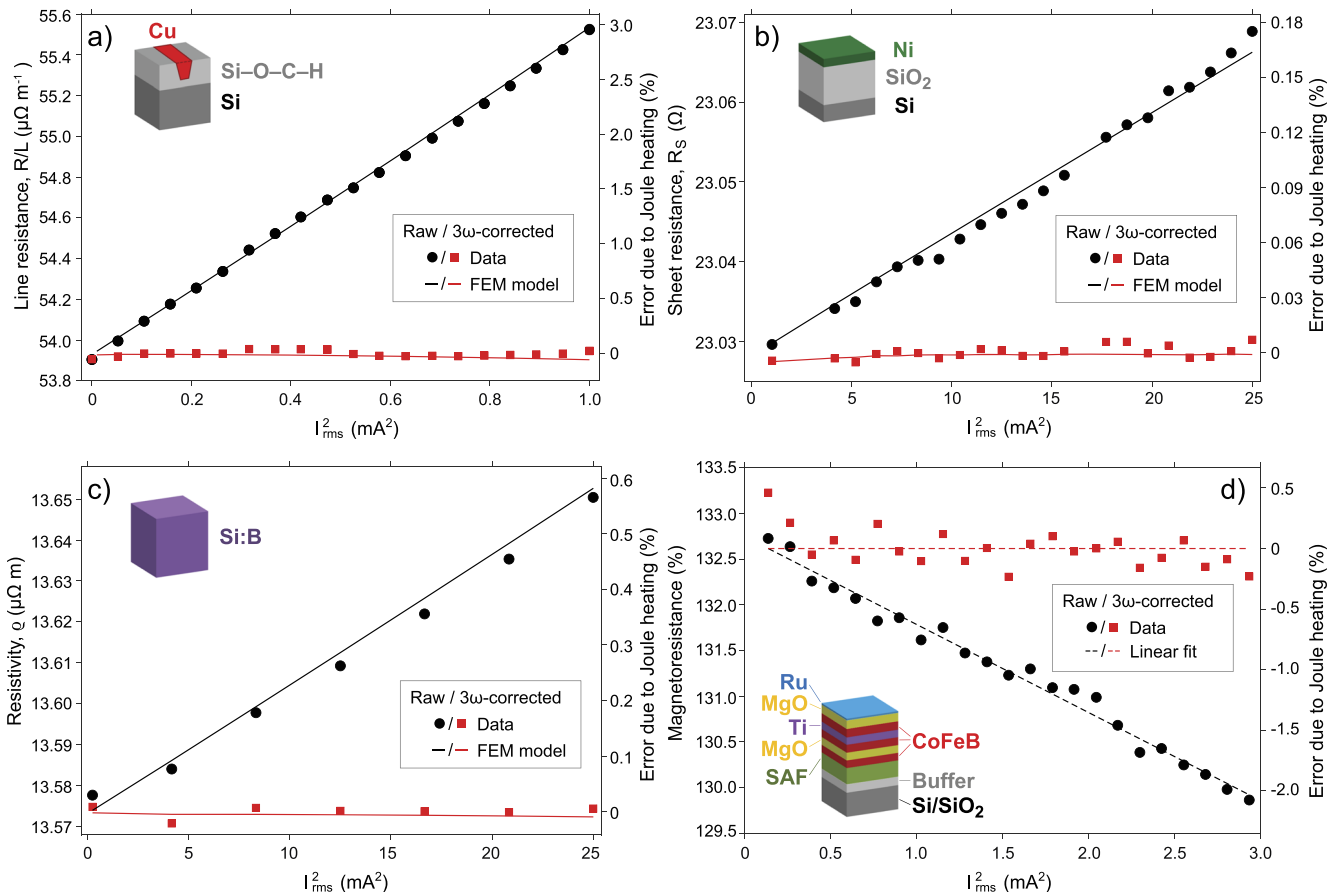


FIG. 2. Raw (circles) and 3ω -corrected [squares, Eq. (7)] line resistance (a), sheet resistance (b), bulk resistivity (c), and magnetoresistance (d) in four industrially relevant devices under test (insets, see Sec. III A for a detailed description of each device). Right y-axes show the measurement error due to Joule heating, which is dominated by the TCR [(a) and (b)] and a combination of the TCR and thermoelectric voltage [(c) and (d)]. Continuous lines in (a)–(c) correspond to FEM best fits to the experimental data; dashed lines in (d) are merely linear fits (as numerical simulation of the MTJ stack was not attempted). Note that the highest currents in each subplot approach the regime for thermal failure of either the probe and/or the device under test.

ultrathin film [Fig. 2(b)], a highly doped semiconductor [Fig. 2(c)], and a magnetic tunneling junction [MTJ], Fig. 2(d)], all of which were characterized by independent techniques as follows:

- Cu nanowires (1D electric domain):** Fabricated via extreme ultraviolet lithography (EUVL), the nanowires are embedded in an 87 nm thick organosilicate glass (OSG) thin film with a dielectric constant of 3.0. The OSG is deposited on top of a structured 775 μm thick Si substrate. The nominal dimensions of the nanowires are 100 μm (L) \times 50 nm (W) \times 77 nm (H), with a sidewall angle of 87° and 450 nm spacing between neighboring wires. The thermal conductivities of both the low-k OSG ($\kappa_{\text{low-k}} = 0.33 \text{ W m}^{-1} \text{ K}^{-1}$) and Si substrate ($\kappa_{\text{Si}} = 150 \text{ W m}^{-1} \text{ K}^{-1}$) were determined using conventional 3ω metrology,² implementing the multilayer matrix formalism.²¹
- Ni thin film (2D electrical domain):** The metallic thin film was fabricated by physical vapor deposition of Ni on 300 mm wafers in a Canon Anelva EC7800 system. The material stack consists of a 10 nm Ni thin film on a 90 nm SiO₂ layer [$\kappa_{\text{SiO}_2} = 0.93 \text{ W m}^{-1} \text{ K}^{-1}$ estimated from Eq. (6) of Ref. 22], deposited on top of a 775 μm thick bulk Si substrate ($\kappa_{\text{Si}} = 150 \text{ W m}^{-1} \text{ K}^{-1}$ as mentioned above).
- Bulk Si:B (3D electrical domain):** The sample is a Czochralski-grown, industrial-grade, boron-doped silicon wafer ($\varnothing = 100 \text{ mm}$ in diameter and 550 μm thick). The carrier concentration is spatially uniform and is estimated at $\sim 1 \times 10^{20} \text{ cm}^{-3}$. The thermal conductivity $\kappa_{\text{Si:B}} = 65.3 \text{ W m}^{-1} \text{ K}^{-1}$, diffusivity $D = 41.2 \text{ mm}^2 \text{ s}^{-1}$, and specific heat $c_p = 1585 \text{ J m}^{-3} \text{ K}^{-1}$ of Si:B were determined at the macroscale using the transient plane source technique,²³ yielding characteristically suppressed values for highly doped Si.²⁴ A Seebeck coefficient of $S = 250 \mu\text{V K}^{-1}$ was measured using a custom-built thin film Seebeck measurement system (adapted from Ref. 25). Additionally, we directly estimated the TCR ($\alpha = 2.05 \pm 0.02 \times 10^{-3} \text{ K}^{-1}$ within the range 296–336 K) via M4PP measurements utilizing a portable hotplate with a proportional–integral–derivative (PID) controller.
- Magnetic Tunnel Junction (multi-layered quasi-2D electrical domain):** The sample is an industrially relevant, single-junction stack (cf., Ref. 26) of a spin-transfer torque magnetoresistive random access memory (STT-MRAM). The synthetic antiferromagnet is placed below the tunnel barrier, with a 3 Å Ta spacer between the two CoFeB films composing the free layer and a thin MgO layer on top of the free layer (further capped with 30 Å of Ru to facilitate contact with CAPRES probes²⁷).

B. Instrumentation

Electric resistance measurements at the microscale were performed using a CAPRES microRSP[®]-A300 tool utilizing digital lock-in amplification (LIA).⁷ Specifically, and in contrast to its default (factory) settings of extracting solely the first harmonic,⁷ the proprietary LIA module of the A300 tool (cf., Ref. 28) was programmatically extended to extract the transfer resistance R_{nw} and its phase φ_{nw} up to the third harmonic ($n = 1, 2, 3$) of the input current frequency. This extended LIA module was thoroughly tested against a

manifold of known waveforms as well as benchmarked against an external best-in-class tool (MFLI from Zürich Instruments).

Samples (a)–(c) were characterized using an equidistant probe with a pitch of 8 μm ;⁷ sample (d) with a specialized current-in-plane tunneling (CIPT) probe with varying distances in the 0.5–10 μm range.²⁷ Measurements were performed at low frequencies of $f = 3.01$ [(a) and (b)], 12.06 (c), and 48.22 Hz (d). Lead resistances of all electrodes were monitored, subtracted, and regressed into individual contact resistances, as detailed in Ref. 9.

C. Numerical simulations

While the complexity of simulating an MTJ stack [Fig. 2(d)] goes beyond the scope of this work,^{29,30} all other experimental data [circles and squares in Figs. 2(a)–2(c)] were numerically reproduced [lines in Figs. 2(a)–2(c)] using COMSOL Multiphysics[®].³¹ All models included coupled *electric currents* and *heat transfer in solids* modules; the simulation of sample (c) included *thermoelectric effects* as well. All nominal device dimensions/geometries were accurately reproduced (with domain reduction due to symmetry wherever possible), and all the experimentally obtained physical constants (Sec. III A) were assigned. Model element sizes were on average a factor of 5–10 smaller than the critical dimensions in their vicinity. The initial conditions of potential (0 V) and temperature (300 K) were supplemented by a thermal insulation on the probing surface (the upper plane of each device) and a constant temperature of 300 K on all other external surfaces. In all models, two terminals of opposite polarity were located 8 μm apart, delivering a sinusoidal current through corresponding trapezoidal (a), semicircular (b), and hemispherical (c) contact geometries (with effective contact radii further denoted as r_0). For the metal–semiconductor contacts in (c), an additional thermal flux at each contact (arising from a contact resistance of 50 Ω , obtained experimentally) was added, following the procedure described in Ref. 9. A time-dependent solver was used to simulate the underlying waveforms (64 time points per period) for each of the observation points in Figs. 2(a)–2(c), with numerical tolerance $< 10^{-5}$. Boundary probes (a) or point probes [(b) and (c)] were used to obtain the voltage at the approximated (a) or precise [(b) and (c)] locations of the two sensing electrodes. The voltage harmonics were then extracted using a numerical lock-in amplifier (thoroughly validated against synthetic waveforms). Convergence tests were conducted to verify that the domain size, meshing, and tolerance were adequately selected.

IV. RESULTS AND DISCUSSION

A. De-trending resistivity measurements from self-heating effects

The linear response of line resistance [Fig. 2(a)], sheet resistance [Fig. 2(b)], bulk resistivity [Fig. 2(c)], and magnetoresistance [Fig. 2(d)] as a function of the square of the probing current is ubiquitous in all studied materials, leading to fractional errors of up to a few percent.³² Given that the M4PP method is generally associated with a precision and reproducibility of $< 0.1\%$,³³ self-heating errors of up to a few percent cannot be regarded as negligible and necessitate an adept correction scheme. In contrast, the proposed 3ω correction method, involving a linear combination of the first and third harmonics [Eq. (7)], yields current-insensitive “flat” trends [squares

in Figs. 2(a)–2(d)], whose slopes are statistically indistinguishable from 0 and whose means overlap with the zero-current intercept that may be regressed from the uncorrected measurements.^{10,11}

B. Determination of thermal properties

The trends of the uncorrected measurements [intentionally removed by Eq. (7)] bear valuable information regarding the thermal properties of the sample [which can be utilized by Eq. (8)]. Since the domain-averaged transfer coefficient Ψ [Eq. (2)] may be difficult to evaluate even in the simplest of geometries⁹ and the potential contribution of thermoelectric voltage is not included in Eq. (3), we resort to a fully numerical approach, where we simulate the observed data via the FEM (Sec. III C). The continuous lines in Figs. 2(a)–2(c) are the numerical best fits to the experimental data, yielding the following regressed parameters:

- Cu nanowire*: $R_0/L = 53.93 \mu\Omega \text{ m}^{-1}$, $\alpha = 1.13 \times 10^{-3} \text{ K}^{-1}$, and $r_0 \sim 50 \text{ nm}$.
- Ni thin film*: $R_{S,0} = 22.8494 \Omega$, $\alpha = 3.34 \times 10^{-3} \text{ K}^{-1}$, and $r_0 = 250 \text{ nm}$.
- Bulk Si:B*: $\rho_0 = 13.295 \mu\Omega \text{ m}$, $\alpha = 1.93 \times 10^{-3} \text{ K}^{-1}$, and $r_0 = 125 \text{ nm}$.

The obtained TCR estimates quoted above are in remarkable agreement with the literature. Specifically, the best fit $\alpha = 1.13 \times 10^{-3} \text{ K}^{-1}$ for the 50 nm wide Cu nanowire promptly extends the trend emerging from wider lines (80–330 nm)³⁴ and is also in line with more recent findings.³⁵ The $\alpha = 3.34 \times 10^{-3} \text{ K}^{-1}$ of the Ni thin film is well bracketed by the broad range reported in Ref. 36 and specifically matches the estimate for a 12.3 nm thick Ni film in Ref. 37 (estimated $3.2 \pm 0.4 \times 10^{-3} \text{ K}^{-1}$ from their Fig. 2). Finally, the best-fit $\alpha = 1.93 \times 10^{-3} \text{ K}^{-1}$ of Si:B not only matches its theoretically expected values,^{38,39} but is also within ~6% of its direct and independent M4PP measurement on a hotplate. Our best fit contact radii (r_0), while technically representing a method-specific parameter rather than any useful sample–probe interaction, are nevertheless consistent with scanning electron microscopy estimates (e.g., Ref. 19).

V. CONCLUSION

The gradual miniaturization of microelectronic devices results in the increase of undesirable self-heating effects when these devices are subjected to electrical/electromagnetic probing using the M4PP. Key fingerprints of heating in response to an applied alternating current can be detected in higher harmonics of the measured voltage,^{2,12,13} which are easy to isolate by means of lock-in amplification.⁷ Here, we have presented the theory (Sec. II), experimental proof (symbols in Fig. 2), and numerical verification (lines in Fig. 2) for the use of 3ω voltage signals for de-trending M4PP resistance measurements from self-heating effects. The presented 3ω correction [Eq. (7)] was demonstrated on samples of broadly varying structures and dimensionalities (Fig. 2). In all studied materials, a definitive (percent-level) improvement in accuracy of M4PP measurements was demonstrated. This marks the 3ω correction as yet another qualitative breakthrough in the evolving accuracy of M4PP resistance metrology (cf., Ref. 27).

The success in reproducing both raw and de-trended M4PP observations via FEM simulations supports the applicability of our quasi-DC assumption to the low-frequency range (<50 Hz), within which routine M4PP measurements are typically performed.^{8,9} While an extension of the theory for true AC is highly desirable,² the electrical and thermal fields arising from even the simplest four-point probing geometries are complex⁹ and render such a mathematical treatment significantly beyond the scope of this work. It should be noted that the presented DC-limit correction has been observed to perform well even at higher frequencies of ~400 Hz. Nevertheless, since the cut-off frequency for the proposed 3ω correction depends on a multiplicity of parameters (including, among others, the desired tolerance, probe geometry, material properties, etc.), we are currently hesitant to report a guiding cut-off frequency. Instead, we encourage to explore and set such thresholds for particular case scenarios via sensitivity analysis based on numerical modeling [cf., Figs. 2(a)–2(c)].

We believe that this study solidifies the recently demonstrated capability of the M4PP for TCR metrology,⁹ extending it to a much broader range of materials, device geometries, and electrical dimensionalities (Fig. 2). At the same time, we emphasize that in our current state-of-the-art, the thermal properties obtained from such M4PP measurements are highly model-driven and are not to be mistaken for a straightforward measurand (as transfer resistance is). Nevertheless, we believe that the prospects of the higher harmonic M4PP measurements to complement, overlap, and perhaps even crossover with scanning thermal microscopy techniques^{40,41} are rather self-evident and highly promising.

ACKNOWLEDGMENTS

This work was supported by Innovation Fund Denmark (Grant Nos. 8054-00020B and 8057-00010B) and Independent Research Fund Denmark (Grant No. 8048-00088B). Roel Gronheid and Andrew Cross (KLA) are thanked for coordinating the fabrication of the nanowire sample and Nini Pryds (DTU) for the portable hotplate equipment.

DATA AVAILABILITY

The data and models that comprise Figs. 1 and 2 are available from the corresponding author upon reasonable request.

REFERENCES

- D. G. Cahill, *Rev. Sci. Instrum.* **61**, 802 (1990).
- C. Dames and G. Chen, *Rev. Sci. Instrum.* **76**, 124902 (2005).
- C. L. Petersen, F. Grey, I. Shiraki, and S. Hasegawa, *Appl. Phys. Lett.* **77**, 3782 (2000).
- D. C. Worledge, *Appl. Phys. Lett.* **84**, 1695 (2004).
- R. Lin, P. Bøggild, and O. Hansen, *J. Appl. Phys.* **96**, 2895 (2004).
- D. H. Petersen, O. Hansen, T. M. Hansen, P. Bøggild, R. Lin, D. Kjær, P. F. Nielsen, T. Clarysse, W. Vandervorst, E. Rosseel, N. S. Bennett, and N. E. B. Cowern, *J. Vac. Sci. Technol., B* **28**, C1C27 (2010).
- P. F. Nielsen, D. H. Petersen, R. Lin, A. Jensen, H. H. Henriksen, L. Gammelgaard, D. Kjær, and O. Hansen, in *Proceedings of the 12th International Workshop on Junction Technology* (IEEE, 2012), p. 1; available at <https://ieeexplore.ieee.org/abstract/document/6212819>.
- J. Bogdanowicz, S. Folkersma, S. Sergeant, A. Schulze, A. Moussa, D. H. Petersen, O. Hansen, H. H. Henriksen, P. F. Nielsen, and W. Vandervorst, *Phys. Status Solidi A* **215**, 1700857 (2018).

- ⁹T. A. Marangoni, B. Guralnik, K. A. Borup, O. Hansen, and D. H. Petersen, *J. Appl. Phys.* **129**, 165105 (2021).
- ¹⁰J. L. Riddle, G. T. Furukawa, and H. H. Plumb, *Nat. Bureau Stand.* **126**, 1 (1973); available at <https://searchworks.stanford.edu/view/10766229>.
- ¹¹V. Batagelj, J. Bojkovski, and J. Drnovšek, *Meas. Sci. Technol.* **14**, 2151 (2003).
- ¹²M. Cutler, *J. Appl. Phys.* **32**, 1075 (1961).
- ¹³M. Cutler, *Adv. Energy Convers.* **2**, 29 (1962).
- ¹⁴R. G. Mazur and D. H. Dickey, *J. Electrochem. Soc.* **113**, 255 (1966).
- ¹⁵M. M. Waldrop, *Nature* **530**, 144 (2016).
- ¹⁶J. He and T. M. Tritt, *Science* **357**, 6358 (2017).
- ¹⁷K. Serbulova and Y. Vountesmery, in *IEEE 39th International Conference on Electronics and Nanotechnology* (IEEE, 2019), p. 369.
- ¹⁸D. C. Gupta and J. Y. Chan, *Rev. Sci. Instrum.* **41**, 176 (1970).
- ¹⁹T. Ansbaek, D. H. Petersen, O. Hansen, J. B. Larsen, T. M. Hansen, and P. Bøggild, *Microelectron. Eng.* **86**, 987 (2009).
- ²⁰D. W. Koon, F. Wang, D. H. Petersen, and O. Hansen, *J. Appl. Phys.* **114**, 163710 (2013).
- ²¹B. W. Olson, S. Graham, and K. Chen, *Rev. Sci. Instrum.* **76**, 053901 (2005).
- ²²T. Yamane, N. Nagai, S.-i. Katayama, and M. Todoki, *J. Appl. Phys.* **91**, 9772 (2002).
- ²³M. Gustavsson, E. Karawacki, and S. E. Gustafsson, *Rev. Sci. Instrum.* **65**, 3856 (1994).
- ²⁴Y. Lee and G. S. Hwang, *Phys. Rev. B* **86**, 075202 (2012).
- ²⁵S. Iwanaga, E. S. Toberer, A. LaLonde, and G. J. Snyder, *Rev. Sci. Instrum.* **82**, 063905 (2011).
- ²⁶H. Sato, M. Yamanouchi, S. Ikeda, S. Fukami, F. Matsukura, and H. Ohno, *Appl. Phys. Lett.* **101**, 022414 (2012).
- ²⁷A. Cagliani, F. W. Østerberg, O. Hansen, L. Shiv, P. F. Nielsen, and D. H. Petersen, *Rev. Sci. Instrum.* **88**, 095005 (2017).
- ²⁸Stanford Research Systems Manual, “Model SR830 DSP Lock-In Amplifier,” 2005, www.thinksrs.com.
- ²⁹D. H. Lee and S. H. Lim, *Appl. Phys. Lett.* **92**, 233502 (2008).
- ³⁰X. Zhang, G. Zhang, L. Shen, P. Yu, and Y. Jiang, *Solid-State Electron.* **173**, 107878 (2020).
- ³¹COMSOL Multiphysics[®], v. 5.6., www.comsol.com, COMSOL AB, Stockholm, Sweden.
- ³²Massive errors of up to ~20%, observed in bulk Bi₂Te₃, will be reported elsewhere.
- ³³D. Kjaer, R. Lin, D. H. Petersen, P. M. Kopalidis, R. Eddy, D. A. Walker, W. F. Egelhoff, and L. Pickert, *AIP Conf. Proc.* **1066**, 167 (2008).
- ³⁴Q. Huang, C. M. Lilley, M. Bode, and R. Divan, *J. Appl. Phys.* **104**, 023709 (2008).
- ³⁵R. S. Smith, E. T. Ryan, C.-K. Hu, K. Motoyama, N. Lanzillo, D. Metzler, L. Jiang, J. Demarest, R. Quon, L. Gignac, C. Breslin, A. Giannetta, and S. Wright, *AIP Adv.* **9**, 025015 (2019).
- ³⁶R. B. Belser and W. H. Hicklin, *J. Appl. Phys.* **30**, 313 (1959).
- ³⁷J. W. C. De Vries, *Thin Solid Films* **150**, 209 (1987).
- ³⁸P. W. Chapman, O. N. Tufte, J. D. Zook, and D. Long, *J. Appl. Phys.* **34**, 3291 (1963).
- ³⁹W. M. Bullis, F. H. Brewer, C. D. Kolstad, and L. J. Swartzendruber, *Solid-State Electron.* **11**, 639 (1968).
- ⁴⁰T. Borca-Tasciuc, *Annu. Rev. Heat Transfer* **16**, 211 (2013).
- ⁴¹Y. Zhang, W. Zhu, F. Hui, M. Lanza, T. Borca-Tasciuc, and M. Muñoz Rojo, *Adv. Funct. Matter* **30**, 1900892 (2020).